Collective gradient sensing by swimming bacteria without clustering

Tatsuro Kai,[1,*] Takahiro Abe,[1,*] Natsuhiko Yoshinaga,[2,3] Shuichi Nakamura,[1] Seishi Kudo,[1] and Shoichi Toyabe[1,†]

[1] *Department of Applied Physics, Graduate School of Engineering, Tohoku University, 980-8579 Sendai, Japan.*
[2] *WPI Advanced Institute for Materials Research, Tohoku University, 980-8577 Sendai, Japan.*
[3] *MathAM-OIL, AIST, 980-8577 Sendai, Japan.*

(Dated: November 18, 2022)

We demonstrate that bacterial cells enhance the taxis performance by collective migration originating from the cellular alignment interaction without apparent clustering. We confine *Salmonella* cells in a shallow channel and evaluate the thermotaxis response to local heating and diffusion. By combining cell tracking analysis and numerical simulation based on simple modeling, we show that the alignment interaction suppresses orientation fluctuation, strengthens migration bias, and also prevents the dispersion of accumulated population. The results show a prominent example of how a collective motion of active matter implements a biological function.

Nearly all bacterial species implement the taxis ability to migrate along the gradient of, for example, chemicals and temperature to seek a better environment. The mechanism underlying taxis differs from species to species. Bacteria with peripheral flagella such as *Escherichia coli* and *Salmonella* exhibit biased random walk with alternative run and tumble motions [1] [Fig. 1(a)]. Signal-dependent modulation of the tumbling frequency enables taxis. However, since such trial-and-error swimming of individual cells is highly stochastic, the taxis efficacy is not expected to be high. On the other hand, it is known that bacteria suspended at high density swim collectively and exhibit rich spatiotemporal phenomena such as long-distance ordering [2, 3], giant number fluctuations [2], and vortex formation [4, 5] caused by interaction among cells. A question that naturally arises is how the cellular interaction affects the taxis performance.

Previous work showed that the chemotaxis performance of swimming [6] and swarming cells [7] increases with the cell density, implying that cellular interaction enhances taxis. However, the enhancement mechanism has remained elusive. This work aims to clarify the mechanism of how cellular interaction modifies taxis. For this aim, we study a low-density cell suspension ($\sim 1\,\mathrm{cell}/100\mu\mathrm{m}^2$) of *Salmonella enterica* cells, where apparent clustering is not observed. As well, we exploit dynamic local heating by laser irradiation and measure the initial taxis dynamics before cells locally accumulate.

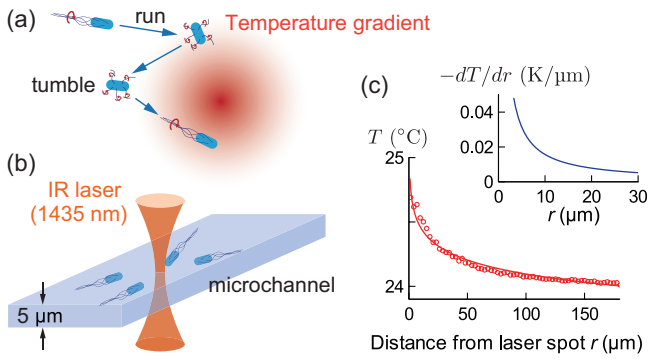

FIG. 1. Bacterial taxis. (a) Stochastic run and tumble motion realizes taxis. (b) Experimental setup. An infrared (IR) laser was focused under a microscope to generate a temperature gradient in a microchannel [Fig. S1]. (c) Temperature gradient generated by local laser heating with 200 mW power. The profile was well fitted by $a - b \ln r$ with $a = 24.8$ and $b = 0.157$. r is the distance from the laser spot. The inset is the gradient calculated as b/r. See Fig. S2 for details.

At a low density, the taxis may be evaluated based on a framework similar to that for the thermophoresis of non-active microscopic objects [8]. Let $c(\vec{r}, t)$ be the particle density at position $\vec{r}$ and time t. Under a given temperature gradient $\vec{\nabla} T$, both the taxis and the thermophoretic flow of non-active particles are phenomenologically described as

$$\vec{J} = D_{\mathrm{T}}(c) c \vec{\nabla} T - D(c) \vec{\nabla} c \tag{1}$$

in a linear-response regime. D_{T} and D are thermodiffusion and diffusion coefficients, respectively. The balance between migration bias and diffusion quantified by the Soret coefficient $S_{\mathrm{T}} \equiv D_{\mathrm{T}}/D$ determines the efficacy of detecting the temperature gradient. Actually, if the dependence of D_{T} and D on c are negligible, we obtain the steady distribution $c \propto e^{S_{\mathrm{T}} T}$ by solving $\vec{J} = 0$. This is often the case for thermophoresis. The phoresis and taxis have distinct origins. The thermophoresis is basically driven by the interaction between the particle surface and solvent [9], whereas bacteria realize thermotaxis by modulating their swimming pattern based on biochemical responses to a thermal gradient[1]. Bacteria swim ballistically at a short time scale and effectively exhibit diffusional motion only at a long time scale[1]. Despite these differences, it would be still effective to evaluate the taxis efficacy based on $D_{\mathrm{T}}(c)$, the effective diffusion coefficient $D^{\mathrm{eff}}(c)$, and their ratio $S_{\mathrm{T}}^{\mathrm{eff}}(c) \equiv D_{\mathrm{T}}(c)/D^{\mathrm{eff}}(c)$.

We observed the swimming cells confined in a thin microchannel with the height of $h = 5\,\mu\mathrm{m}$, which is comparable to the cell dimensions (2–3μm in length and $\sim 1\,\mu\mathrm{m}$ in width) [Fig. 1(b)]. Cells may pass each other. However, since vertical swimming is negligible, we treat the system as two-dimensional and evaluate c, D_{T}, and

$D^{\rm eff}$ as two-dimensional quantities. Irradiation of focused infrared laser under a microscope generated an axisymmetric pseudo-two-dimensional temperature gradient [10, 11]. This setup enables the instantaneous switching on and off of the gradient for probing the taxis dynamics. The thermal convection due to the local heating was negligible because of the reduced channel height. The consumption of nutrients by cells creates a nutrient gradient and makes the dynamics complex [11, 12]. We used the observation buffer lacking nutrients to focus on the effect of the cellular interaction on taxis. We also evaluated $D_{\rm T}$ using the initial migration speed since cellular respiration may form the spatial oxygen gradient at a later time. The magnitude of interaction was controlled by varying the cell density.

Results – taxis. The spatial temperature profile under local laser heating was well fitted by a logarithmic function as expected from the two-dimensional open system with a single heat source[13] [Fig. 1(c)]. The maximum temperature increase was about 0.7 K.

The cells migrated along the temperature gradient $\vec{\nabla}T$ and accumulated in the vicinity of the heating spot [Figs. 2(a), S5], indicating $D_{\rm T} > 0$ under the present condition. The cells dispersed when the laser was turned off. The mutant strains without flagella (fla-) nor Che system (che- [14]) did not accumulate significantly [Fig. S6]. The che- strain produces an intact flagellar apparatus but rotates its motors exclusively counter-clockwise without tumbling. Hence, the migration originates in the taxis, not in the optical-tweezers effect [15] nor the thermophoresis [8].

Let $c_R(t)$ be the mean cell density in the vicinity of the heating spot (the region within $R = 50\,\mu$m) and c_0 be the mean cell density in the same region before the laser is turned on. c_0 was typically in the order of 1 cell/100μm^2. The normalized cell density $c_R(t)/c_0$ increased linearly with a short time delay and saturated with the timescale of $\sim$ 80 s [Fig. 2(b)]. The short delay was supposedly caused by the response delay of individual cells and the large R we used.

The increase in c_R should equal the influx through the region's boundary. The magnitude of the influx is obtained by integrating the radial component J_r of $\vec{J}$ at the peripheral, $\dot{c}_R = 2\pi R J_r/\pi R^2$. Initially, $|\vec{\nabla}c|$ is negligible because of the uniform cell density. Hence, (1) is reduced to $\vec{J} = D_{\rm T} c \vec{\nabla}T$, which leads to $\dot{c}_R = 2D_{\rm T}c_0|\vec{\nabla}T|_R/R$. Here, $|\vec{\nabla}T|_R = 0.0031\,$K/μm is the temperature gradient at R. Thus, we can evaluate $D_{\rm T}$ as $D_{\rm T} = \alpha \dot{c}_R(t_0)/c_0$ with $\alpha = 0.5R/|\vec{\nabla}T|_R = 8.0 \times 10^3\,\mu{\rm m}^2{\rm K}^{-1}$. Here, $t_0 = 30\,$s is the time that the laser irradiation starts. We fitted the time profile of $c_R(t)$ during heating by an exponential curve and evaluated $\dot{c}_R(t_0)$. We excluded the first 10 s during heating from the fitting range to remove the effect of the short time delay of $c_R(t)$ rising. We found that $D_{\rm T}$ increases with c_0. Since the increase in c_0 increases the contact frequency of cells, the results imply that the cellular interaction enhances taxis [Fig. 2(c)].

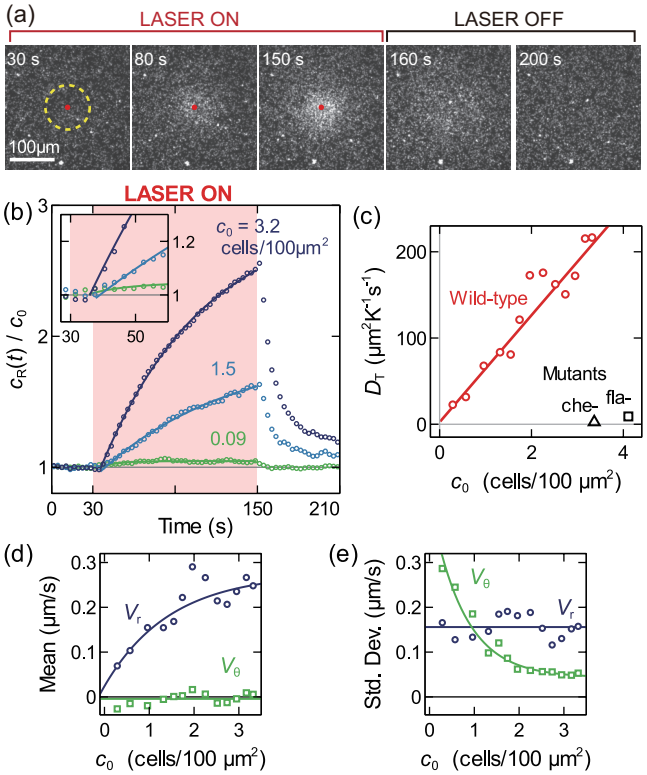

FIG. 2. Taxis to local heating. (a) The snapshots of the migration at $c_0 = 2.5\,$cells/100μm^2 were observed by dark-field microscopy. The red dot indicates the laser irradiation location. (b) The normalized cell density $c_R(t)/c_0$ in the central region within $R = 50\,\mu$m indicated as a yellow dotted circle in (a). $c_R(t)/c_0$ was evaluated as the ratio of the light intensity scattered by the cells under dark-field microscopy. c_0 was separately evaluated by phase-contrast microscopy. The data are fitted by exponential curves (solid lines) in the range between 40 s and 150 s. The time profiles of 20 runs with similar c_0 are averaged. (c) Dependence of $D_{\rm T}$ on c_0. The solid curve is a linear fitting. The number of independent observations is 141. We divided the runs sorted by c_0 into groups containing 20 runs with 10-run overlaps and calculated quantities in each group. (d, e) Single-cell tracking. The mean (d) and standard deviation (e) of radial ($V_{\rm r}$) and angular (V_θ) components of the velocity under the local heating averaged in the distance range between 74 and 198 μm from the heating spot and the time range of between 40 and 70 s. See SI Method for details. Each point is obtained from 20 runs. The solid curves are exponential or constant fittings. The plot was limited to $c_0 > 0.1\,$cell/100μm^2 due to limited sample number at low c_0.

For further characterization of migration dynamics, we tracked individual cells and evaluated the radial ($V_{\rm r}$) and angular (V_θ) components of the swimming velocity [Fig. 2(d, e)]. Since it was not feasible to track all the cells due to their overlaps, the analysis was limited to a subset of the entire population. The mean of $V_{\rm r}$ increases with c_0 while the standard deviations of V_θ decrease with c_0,

implying that the cellular interaction strengthened the directional bias toward the heating spot.

Results – cellular interaction. The above results indicate that cellular interaction enhances the taxis. To characterize the interaction, we analyzed the collision angles $\theta_{\rm in}$, $\theta_{\rm out}$, and their difference $\Delta\theta = \theta_{\rm out} - \theta_{\rm in}$ in the absence of thermal gradient [Fig. 3] [3, 16–18].

The cells aligned after collisions with $\theta_{\rm in} < 45°$ and did not significantly align otherwise. Such mixed asymmetric interaction of polar and nematic types has been observed for the binary collision of the objects that can pass each other [18].

Results – diffusion. Next, we evaluated how the modulation of diffusion by cellular interaction affects the taxis. After the laser was turned off, the cells dispersed quickly in an exponential manner [Fig. 2b]. The time constant of the dispersion $\tau_{\rm dis}$ increased with c_R at the timing of laser off [Fig. S8]. We expect $\tau_{\rm dis}$ to be independent of the density for passive Brownian particles unless the particles are extremely dense. The result implies that the cellular interaction modulates diffusion.

For more characterization, we tracked the diffusion of individual cells without laser heating. In order to track a long trajectory at high cell density, we mixed cells expressing green fluorescent protein (GFP). We first measured c_0 by counting cells in phase-contrast observation and then quantified the diffusion using the GFP cells in the same observation area in succession.

The run and tumble motion generated ballistic and diffusive motions at short and long time scales, respectively [Fig. 4(a)]. Trajectories became more diffusive at higher c_0, implying the modulation of the swimming pattern by the cellular interaction.

The mean square displacement (MSD), $M(\Delta t) \equiv \langle|\vec{r}(t+\Delta t)-\vec{r}(t)|^2\rangle_t$, characterizes the diffusion [Fig. 4(b)]. Here, the average $\langle\cdot\rangle_t$ is taken for different t. The effective diffusion coefficient $D^{\rm eff}$ is defined in the long Δt limit as $D^{\rm eff} = \lim_{\Delta t\to\infty} M(\Delta t)/4\Delta t$ in two dimensional

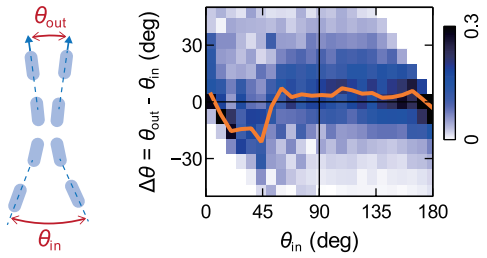

FIG. 3. Alignment interaction quantified by the angular displacement by collision. We used the same data as that in Fig. 4 ($h = 5\,\mu$m and $c_0 < 1.5\,$cells/100μm^2). We analyzed 11,823 events where two cells come to close in a distance less than 2.2 μm. See SI for the details. The color intensity indicates the frequency of the collision events normalized in each column. The solid line indicates the peak locations of the skewed normal distributions fitted in each column.

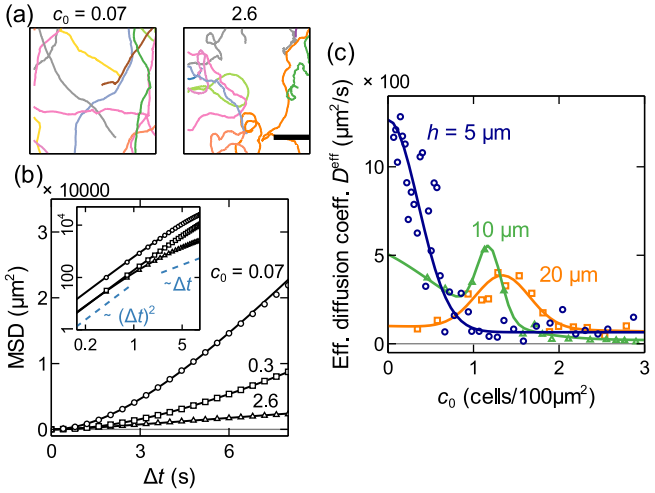

FIG. 4. Diffusion in the absence of temperature gradient. (a) Two-dimensional trajectories in the chamber with the height of $h = 5\,\mu$m. The scale bar indicates 100 μm. (b) The mean square displacement (MSD) curve in the chamber with the height of $h = 5\,\mu$m. The values of c_0 are indicated in the unit of cells/100μm^2. The inset is the log-log plot. (c) Effective diffusion coefficient $D^{\rm eff}$. The solid curves are fitting curves (see section V of SI). The numbers of independent observations are 389, 120, and 192 for $h = 5$, 10, and 20 μm, respectively. The runs sorted by c_0 are divided into groups of 10 ($h = 5\,\mu$m), 8 (10 μm), or 12 (20 μm) runs and analyzed collectively in each group.

systems. Since trajectories accessible by experiments are relatively short, we exploited a model fitting for estimating $D^{\rm eff}$. The MSD of a self-propelled particle with random directional change is described by

$$M(\Delta t) = 2v^2\tau\left[\Delta t - \tau(1 - e^{-\Delta t/\tau})\right] \qquad (2)$$

for a broad range of systems [19–21] including a run-and-tumble motion. Here, v is the swimming velocity, and τ is the mean duration between successive direction changes. In the present system, the change in direction is supposed to be caused by the tumbling and the cellular interaction. At large Δt, $M(\Delta t) \simeq 2v^2\tau\Delta t$, which yields $D^{\rm eff} = v^2\tau/2$. We fitted $M(\Delta t)$ by (2) to obtain $D^{\rm eff}$.

$D^{\rm eff}$ decreased with c_0 as expected from the increase in diffusive motions. τ significantly decreased with c_0, whereas clear dependence of v on c_0 was not observed [Fig. S9]. Thus, the cells change directions more frequently at higher c_0. The result is consistent with the extended dispersion time after the laser is off at high cell density [Fig. S8]. Once accumulated, the cells disperse slowly due to the slow diffusion caused by cell-cell interaction. These results indicate that the taxis enhancement by cell interaction is caused by both the increased migration bias and suppressed diffusion at the accumulated region.

We also measured $D^{\rm eff}$ in thicker channels with $h = 10$ and 20 μm as the references. At small c_0, $D^{\rm eff}$ decreased

with h. It is possible that the confinement to a shallow channel suppresses the directional change and enhances the speed. Interestingly, we observed nonmonotonic dependence of $D^{\rm eff}$ on c_0 in the 10- and 20-μm channels [Fig. 4(c)]. Such peak was previously observed, but its mechanism has remained to be unclear [22].

This characteristic may be explained as follows. The alignment interaction suppresses the directional fluctuations and enhances the ballistic motion, which increases $D^{\rm eff}$. However, at high c_0, due to the frequent collisions among cells and long-range hydrodynamic interaction, the correlated swimming may be destabilized. The balance between the alignment and destabilization may shape the peak of $D^{\rm eff}(c_0)$. In the thick channels, cells can easily pass each other, and the destabilization would not be effective unless c_0 is very large. Therefore, the peak position may shift to a large c_0 region. Note that, due to the limited focal depth, c_0 in 10- and 20-μm channels may be underestimated. However, this does not qualitatively affect the conclusion.

Results – Soret coefficient. The effective Soret coefficient $S_{\rm T}^{\rm eff} = D_{\rm T}/D^{\rm eff}$ increased steeply when c_0 exceeds a threshold cell density $c_0^* \sim 1\,{\rm cell}/100\mu{\rm m}^2$ [Fig. 5]. The mean free path at c_0^* is roughly estimated as $\lambda^* = 1/(2dc_0^*) \sim 50\,\mu$m, where $d = 1\,\mu$m is the typical cell width. λ^* is comparable to the size of the heating region [Fig. 1(c)]. This is reasonable because the collective taxis enhancement is not expected if cells do not interact during the migration toward the hot region. The actual value of λ^* should be larger because cells can pass each other even in the present thin chamber. However, λ^* would still be comparable to the heating-spot size.

Results – simulation. For elucidating the mechanism of the taxis enhancement, we modeled the cells as self-propelled spherical particles and performed numerical simulations [Fig. 6] [23–27]. See SI (Section VII) for details. The particles translate with a constant velocity and change their swimming direction by the interaction with other particles as well as rotational fluctuation with white Gaussian statistics. The interaction includes the short-range repulsion, which models the excluded volume effect, the polar interaction, which aligns the swimming direction of nearby cells, and the long-range hydrodynamic interaction, in which the cells are modeled as pushers. We also include the driving by an external field for measuring response.

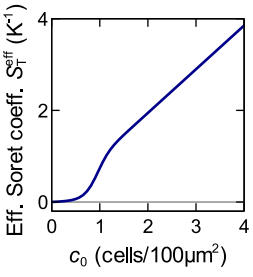

FIG. 5. Effective Soret coefficient $S_{\rm T}^{\rm eff} = D_{\rm T}/D^{\rm eff}$ in the 5-μm chamber calculated based on the fitting curves of Figs. 2(c) and 4(c).

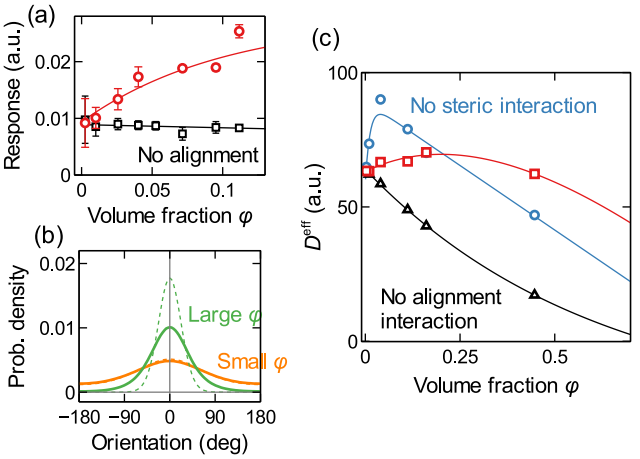

FIG. 6. Simulation. (a) Response to a Gaussian-shaped axisymmetric external field. The solid curves are exponential fitting. (b) Steady distribution of velocity orientation obtained by simulations (solid lines) and mean-field approximation (dashed lines). Uniform external field is induced in the direction of $\theta = 0$. $\varphi = 0.11$ (green) or 0.0025 (orange). (c) Effective diffusion coefficient with/without steric repulsion and polar interaction. The solid curves are exponential+linear (blue and red) or exponential (black) fitting. See also Fig. S4 for the effective Soret coefficient.

The simulations qualitatively reproduced the taxis and diffusion observed in the experiments despite the simplicity of the model [Fig. 6]. Specifically, the response to an external field increased with the initial particle density measured by the volume fraction φ [Fig. 6(a)]. Such density dependence was not observed without alignment interaction. When a uniform external field was imposed, the steady distribution of the orientation became steeper with φ [Fig. 6(b)]. This result reproduced the experimental results [Fig.2(d, e)], validating the hypothesis that the alignment interaction enhances the migration bias and suppresses the rotational diffusion.

The simulation reproduced the peak of $D^{\rm eff}$ observed in experiments [Fig. 6(c)]. Without alignment, $D^{\rm eff}$ monotonically decreased, validating that the alignment interaction enhances the diffusion. The diffusion peak was large without the excluded volume effect, where the particles pass each other. This situation models the experiments with thick chambers, in which we observed prominent peaks [Fig. 4(c)]. Let the cell volume be $3\,\mu{\rm m}^3$. A typical cell density in the experiment $c_0 = 1\,{\rm cell}/100\mu{\rm m}^2$ is converted to the volume fraction of $\varphi = 0.006$ for $h = 5\,\mu$m channel. However, since the interaction range rather than particle size affects the cellular interaction more, it is not straightforward to compare c_0 and φ.

Discussion. Bacterial thermotaxis has been investi-

gated since 1970s [28–30]. The density dependence of the thermotaxis was recently studied with a focus on the effect of the cellular metabolism [11, 12, 31, 32]. Cells' secretion and consumption of chemicals such as glycine and oxygen create a chemical gradient, which induces chemotaxis and modulates the migration. Swimming speed variation by temperature also induces a temperature-dependent diffusion and enables a thermotaxis without receptors for taxis [32].

Here, we circumvented such complication and focused on how the cellular physical interaction affects the taxis behavior. The enhanced migration bias we demonstrated may be explained by a majority voting mechanism. The taxis of a single cell is not effective due to strong fluctuations. However, in a bacterial suspension, cellular interaction aligns the swimming directions of the nearby cells to their major direction and increases the sensing limit.

The collective gradient sensing of migrating eukaryotic cells and animals has been extensively studied [33, 34], where cluster formation is critical. A cluster may be regarded as a large body, which makes it easier to sense a gradient or enables gradient sensing even if individuals are able to sense only a concentration instead of a gradient. On the other hand, the mechanism demonstrated here does not rely on clustering, implying a new class of collective sensing mechanisms.

We thank Yusuke T. Maeda, Tetsuya Hiraiwa, and Yohei Nakayama for helpful discussions and Mao Fukuyama and Akihide Hibara for technical assistance. This research was supported by JSPS KAKENHI (JP18H05427 to ST and JP20K03874 to NY) and Tohoku University Nanotechnology Platform sponsored by MEXT, Japan (JPMX09F-20-TU-0083).

* These authors contributed equally.
† toyabe@tohoku.ac.jp

[1] H. C. Berg, *E. coli in Motion* (Springer, ADDRESS, 2004).
[2] H. P. Zhang, A. Be'er, E.-L. Florin, and H. L. Swinney, Proc. Nat. Acad. Sci. **107**, 13626 (2010).
[3] D. Nishiguchi, K. H. Nagai, H. Chaté, and M. Sano, Phys. Rev. E **95**, (2017).
[4] C. Dombrowski, L. Cisneros, S. Chatkaew, R. E. Goldstein, and J. O. Kessler, Phys. Rev. Lett. **93**, (2004).
[5] K. Beppu, Z. Izri, J. Gohya, K. Eto, M. Ichikawa, and Y. T. Maeda, Soft Matter **13**, 5038 (2017).
[6] R. Colin, K. Drescher, and V. Sourjik, Nature Communications **10**, (2019).
[7] M. Tian, C. Zhang, R. Zhang, and J. Yuan, Biophys. J. **120**, 1615 (2021).
[8] R. Piazza and A. Parola, J. Phys. **20**, 153102 (2008).
[9] J. L. Anderson, Ann. Rev. Fluid Mech. **21**, 61 (1989).
[10] D. Braun and A. Libchaber, Phys. Rev. Lett. **89**, (2002).
[11] M. Demir, C. Douarche, A. Yoney, A. Libchaber, and H. Salman, Phys. Biol. **8**, 063001 (2011).
[12] H. Salman, A. Zilman, C. Loverdo, M. Jeffroy, and A. Libchaber, Phys. Rev. Lett. **97**, (2006).
[13] Y. Sakamoto and S. Toyabe, Sci. Rep. **7**, (2017).
[14] Y. Magariyama, S. Yamaguchi, and S. Aizawa, J. Bacteriol. **172**, 4359 (1990).
[15] A. Ashkin, Proc. Nat. Acad. Sci. **94**, 4853 (1997).
[16] I. S. Aranson, A. Sokolov, J. O. Kessler, and R. E. Goldstein, Phys. Rev. E **75**, (2007).
[17] T. Ishikawa, J. Roy. Soc. Interface **6**, 815 (2009).
[18] R. Suzuki, C. A. Weber, E. Frey, and A. R. Bausch, Nature Physics **11**, 839 (2015).
[19] X. Wu and A. Libchaber, Phys. Rev. Lett. **84**, 3017–3020 (2000).
[20] J. R. Howse, R. A. L. Jones, A. J. Ryan, T. Gough, R. Vafabakhsh, and R. Golestanian, Phys. Rev. Lett. **99**, 048102 (2007).
[21] H.-R. Jiang, N. Yoshinaga, and M. Sano, Phys. Rev. Lett. **105**, 268302 (2010).
[22] M. Wu, J. W. Roberts, S. Kim, D. Koch, and M. DeLisa, Appl. Environ. Microbiol. **72**, 4987–4994 (2006).
[23] A. Amiri, R. Mueller, and A. Doostmohammadi, J. Phys. A **55**, 094002 (2022).
[24] E. Sesé-Sansa, D. Levis, and I. Pagonabarraga, Phys. Rev. E **104**, 054611 (2021).
[25] J. Blake, Bull. Aust. Math. Soc. **5**, 255 (1971).
[26] N. Yoshinaga and T. B. Liverpool, Phys. Rev. E **96**, 020603(R) (2018).
[27] T. Hiraiwa, Phys. Rev. Lett. **125**, (2020).
[28] K. Maeda, Y. Imae, J. I. Shioi, and F. Oosawa, J. Bact. **127**, 1039 (1976).
[29] K. Maeda and Y. Imae, Proc. Nat. Acad. Sci. **76**, 91 (1979).
[30] E. Paster and W. S. Ryu, Proc. Nat. Acad. Sci. **105**, 5373 (2008).
[31] H. Salman and A. Libchaber, Nat. Cell Biol. **9**, 1098 (2007).
[32] M. Demir and H. Salman, Biophys. J. **103**, 1683 (2012).
[33] B. A. Camley, J. Phys. **30**, 223001 (2018).
[34] A. Haeger, K. Wolf, M. M. Zegers, and P. Friedl, Trends Cell Biol. **25**, 556 (2015).